Acta Cryst. (1985). A41, 309-316

Small-Crystal X-ray Diffractometry with a Crystal Ante-Monochromator

BY A. MCL. MATHIESON

Division of Chemical Physics, CSIRO, PO Box 160, *Clayton, Victoria, Australia* 3168

(*Received* 9 *April* 1984; *accepted* 28 *November* 1984)

Abstract

A treatment is given in terms of $\Delta\omega$, $\Delta 2\theta^{(s)}$ space of the system involving an X-ray source, a crystal monochromator and a single-crystal diffractometer. The interaction of the wavelength dispersion of the monochromator crystal, *M*, and that of the small specimen crystal, *C*, is examined for various orientations of the axis of *M* relative to that of *C*. A simple diagrammatic representation of the wavelength dispersion of the system is derived. These diagrams encompass the parallel, antiparallel and crossed-crystal arrangements and are equivalent to the theoretical relation

$$\frac{\Delta\omega}{\Delta 2\theta}=\frac{k(\tan\theta_C+\cos\varphi_M\tan\theta_M)}{k(2\tan\theta_C+\cos\varphi_M\tan\theta_M)};$$

$\Delta\omega$ is the angular displacement of *C* and $\Delta 2\theta$ the corresponding displacement in detector space, θ_C the Bragg angle of *C* and θ_M that of *M* while $k=(\Delta\lambda/\lambda)\tan\theta_M$ and φ_M is the angle between the axes of *C* and *M*. From the principle of reciprocity in optics, the functional dependence of the radiation that arrives at the small specimen crystal from an extended source *via* the monochromator is investigated in terms of the mosaic spread of *M*, the depth of beam penetration into *M* and the wavelength band. Combination of the wavelength dispersion and the source size/monochromator mosaicity with the mosaic spread of the specimen crystal yields the corresponding $\Delta\omega$, $\Delta 2\theta^{(s)}$ diagrams. For the case where the rotation axes of the *M* and *C* crystals are parallel, the general form of the intensity distributions is examined for selected values of $\tan\theta_C$ relative to $\tan\theta_M$.

Introduction

Recent studies (Mathieson, 1982, 1984*a*) have explored the intensity distribution associated with an individual Bragg X-ray reflection from a small crystal in terms of $\Delta\omega$, $\Delta 2\theta$ space for a basic experimental set-up consisting of an X-ray source, a specimen crystal and its orienting device (diffractometer) and a detector with a narrow aperture in front of it (or a linear position-sensitive detector).

With the incorporation of an additional component, a crystal monochromator, between the source and the specimen crystal (an ante-monochromator, see Mathieson, 1968), certain features in the experiment are affected, namely the divergence/convergence of the X-ray beam and the wavelength distribution, while a new factor is introduced, the interaction between the dispersion of the monochromator crystal and that of the specimen crystal. It is therefore advisable to extend the analysis so far carried out to investigate the modifying influence of the new component on the intensity distribution, $I(\Delta\omega, \Delta 2\theta^{(0)})$ (for terminology, see Mathieson, 1984*a*). Discussion is restricted to the flat-cone mode of operation in respect of the specimen crystal.

Compared with the non-monochromator case, *e.g.* Alexander & Smith (1962), theoretical discussion of combined monochromator/diffractometer X-ray systems has been rather limited, *e.g.* Ladell & Spielberg (1966), Werner (1972).

Although the monochromator/diffractometer system in neutron diffraction has been dealt with extensively by many workers, *e.g.* Willis (1960), Cooper & Nathans (1967, 1968), Werner (1971), *etc.*, the various treatments have generally been presented in the form of relatively cumbersome formulae with rather limited illustration of their relevance to operational practice. Also, the formulae relate to one-dimensional results where the contributions of the various components have all been compressed into the one dimension and, consequently, are not readily identified in experimental profile measurements. As a result, inferences of potential significance for the X-ray case do not appear to have been derived from the neutron case.

That the two-dimensional viewpoint has advantages in identifying and estimating the various components and in providing improved resolving power has been shown in Mathieson (1982, 1984*a*).

A $\Delta\omega$, $\Delta 2\theta^{(0)}$ study of the neutron diffraction case that included a monochromator component has been recently presented by Schoenborn (1983). While it will be evident that there are certain features in common between that study and this one, the present examination is directed primarily at the X-ray diffraction case. The aim here is to present the analysis mainly in diagrammatic form (as in Mathieson, 1982) so that the relative magnitudes of the components are evident by inspection and any significance of a practical nature that the treatment has will be more readily

0108-7673/85/040309-08$01.50

appreciated by X-ray practitioners and hence will provide an effective guide to the choice of experimental parameters, *e.g.* Mathieson (1984*b*), and the appropriate procedure for the measurement of integrated intensity.

While the matter is discussed in terms of 2D ($\Delta\omega$, $\Delta 2\theta$) space, its relevance for the more conventional usages of 1D ($\Delta\omega$) space should be evident.

General plan

The approach to be taken is to consider first the situations that arise in terms of point sources and crystals (specimen and monochromator) with zero mosaic distribution in order to identify the responses of the various components, *i.e.* their loci in $\Delta\omega$, $\Delta 2\theta^{(0)}$ space. The effects of significant mosaic distribution and of extended sources can then be introduced to establish more realistic situations while allowing identification of the presence of characteristic loci. We shall deal only with the case of $s=0$, *i.e.* no synchronized angular displacement of the detector arm with angular displacement of the specimen crystal. For other scan links, $s=1$ or 2, the corresponding distributions can be derived straightforwardly (see Mathieson, 1982, 1984*a*).

So far as the monochromator crystal is concerned, its axis may be at any angle, φ_M, to the axis of the specimen crystal (see Mathieson, 1968, 1978).

Monochromator axis parallel to the specimen axis

(i) *Point source, one wavelength*

Fig. 1 represents the case of a point source, *S*, emitting radiation of only one wavelength, λ, in relation to monochromator and small specimen crystal, *M* and *C*, respectively, with either zero or non-zero mosaic spreads, μ. The resultant distributions in $\Delta\omega$, $\Delta 2\theta^{(0)}$ space are depicted in Fig. 2 for the various combinations of mosaic spread of *M* and *C*, namely (*a*) $\mu_M=\mu_C=0$, (*b*) $\mu_M=0$, $\mu_C=\mu_2$, (*c*) $\mu_M=\mu_1$, $\mu_C=0$, (*d*) $\mu_M=\mu_1$, $\mu_C=\mu_2$; the lengths of the lines in (*b*) and (*c*) and of the edges of the parallelogram in (*d*) represent outer limits of the distribution.

Since only one wavelength is involved, the question of dispersion does not arise and so $+2\theta_C$ and $-2\theta_C$ are equivalent. The beam convergent on *C* from the monochromator crystal is akin to the source in the non-monochromator case.

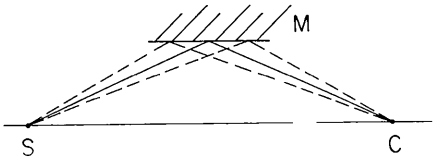

Fig. 1. A point source, *S*, of monochromatic radiation, and a point specimen crystal, *C*, equidistant from the ante-monochromator, *M*.

(ii) *Two point sources, two wavelengths*

Fig. 3 represents the situation with a monochromator crystal, *M*, and a specimen crystal, *C*, both of zero mosaic spread. S_1, S_2 are visualized as separate sources of λ_1, λ_2 respectively or as two points on an extended source, the diffraction conditions at *M* selecting λ_1 and λ_2. Whatever the viewpoint, the situation at the specimen crystal is of two beams, of wavelength λ_1 and λ_2 respectively, converging on the point *C* with an interbeam angle $\Delta\theta_M=\theta_2-\theta_1=(\Delta\lambda/\lambda_1)\tan\theta_M$, where $\Delta\lambda=\lambda_2-\lambda_1$, $\lambda=(1/2)(\lambda_2+\lambda_1)$ and $\theta_M=(1/2)(\theta_2+\theta_1)$. Hereafter, we shall consider the wavelength dispersion, $\Delta\lambda/\lambda=k$, a set value. The incident beams diffract from *C* and, for the post-*C* region, we shall take the beam of λ_1 radiation (the shorter wavelength) as the reference for angle estimation.

The diffraction situation in respect of $\lambda_1\lambda_2$ is no longer symmetrical. Following the convention (in two-crystal spectrometry) that the diffraction from the first (here monochromator) crystal defines the

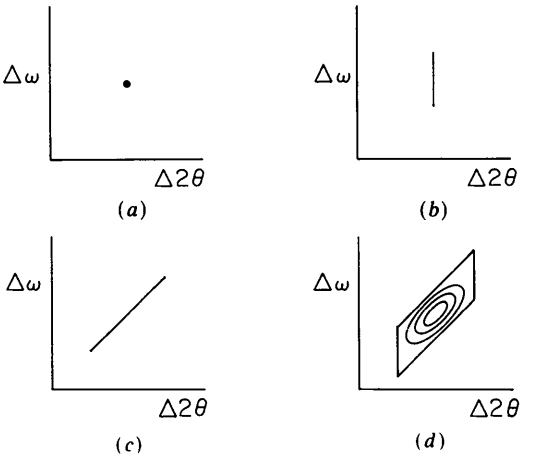

Fig. 2. The hypothetical intensity distributions, $I(\Delta\omega, \Delta 2\theta^{(o)})$, are detailed for the various combinations of mosaic spread of *M* and *C*, namely (*a*) $\mu_M=\mu_C=0$, (*b*) $\mu_M=0$, $\mu_C=\mu_2$, (*c*) $\mu_M=\mu_1$, $\mu_C=0$, (*d*) $\mu_M=\mu_1$, $\mu_C=\mu_2$.

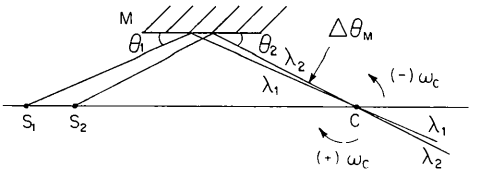

Fig. 3. The situation with two sources S_1 and S_2 of radiation of wavelengths λ_1 and λ_2 respectively, diffracted at angles θ_1 and θ_2 from the monochromator, *M*. At the position of the specimen crystal, *C*, the interbeam angle $\Delta\theta_M=\theta_2-\theta_1$ ($=\Delta\lambda/\lambda\tan\theta_M$), where $\Delta\lambda=\lambda_2-\lambda_1$, $\lambda=(1/2)(\lambda_2+\lambda_1)$ and $\theta_M=(1/2)(\theta_2+\theta_1)$. The positive and negative directions of ω_C are, according to the convention in two-crystal spectrometry, indicated as $(+)\omega_C$ and $(-)\omega_C$.

positive angular direction, then the positive and negative directions of ω_C, $(+)\omega_C$ and $(-)\omega_C$ respectively, follow, see Fig. 3.

(a) The $(-)\omega_C$ region

The 'illumination' distribution, $I(\lambda)$, arriving at the point C, has an angular separation between λ_1 and λ_2 of $\Delta\theta_M = k \tan \theta_M$. This distribution is constant for a given θ_M and invariant in orientation relative to C. The corresponding 'receptor/transmitter' distribution, $R/T(\lambda)$, of C can be displaced around the axis of C and, in addition, the distribution alters with the value of the particular d spacing of the Bragg reflection of C, the separation between λ_1 and λ_2 being $\Delta\theta_C = k \tan \theta_C$.

For the $(-)\omega_C$ region (*i.e.* anti-clockwise rotation of crystal C in Fig. 3), to change the situation in which M and C are set to satisfy the Bragg condition for λ_1 to that for λ_2, *i.e.* to change the coincidence of $R/T(\lambda_1)$ with $I(\lambda_1)$ to the coincidence of $R/T(\lambda_2)$ with $I(\lambda_2)$ requires an angular displacement of the specimen crystal of

$$\Delta\omega = \Delta\theta_C - \Delta\theta_M = k(\tan \theta_C - \tan \theta_M). \quad (1)$$

The corresponding displacement in $\Delta 2\theta$ (detector space) is

$$\Delta 2\theta = \Delta 2\theta_C - \Delta\theta_M = k(2 \tan \theta_C - \tan \theta_M). \quad (2)$$

So the ratio of $\Delta\omega$ to $\Delta 2\theta$ is given by

$$\frac{\Delta\omega}{\Delta 2\theta} = \frac{k(\tan \theta_C - \tan \theta_M)}{k(2 \tan \theta_C - \tan \theta_M)}. \quad (3)$$

Equation (3) establishes, in $\Delta\omega, \Delta 2\theta$ space, (a) the locus of the wavelength component (k) for specific values of θ_M and θ_C and (b) the locus of a constant value of k (and θ_M) with change of θ_C.

The relationship summarized in (3) is more readily appreciated in diagrammatic form, Fig. 4(a). The origin of local $\Delta\omega, \Delta 2\theta$ space for any reflection is arbitrary but, for the present discussion, we associate it with the lower limit of the λ range, namely λ_1. The location of the point corresponding to the upper limit of the λ range, *i.e.* λ_2, follows from (3). So, for fixed values of θ_M and θ_C, *i.e.* for one reflection of the specimen crystal, the locus of the wavelength component is a straight line, for example, OL' in Fig. 4(a), corresponding to a general $\tan \theta_C$ value. For a set value of k, the locus of λ_2 in respect of all reflections of the specimen crystal, *i.e.* as $\tan \theta_C$ varies from 0 to ∞, is represented by the line $O'A'B'C'$.

In dealing with $\Delta\omega, \Delta 2\theta$ space, we have to consider angular dispersion in terms of both $\Delta\omega$ and $\Delta 2\theta$ - not merely $\Delta\omega$, as in the classical wide-aperture treatment. From the 2D viewpoint, there are two conditions of interest, rather than one, as in the classical viewpoint.

At $\theta_C = 0°$, *i.e.* $\tan \theta_C = 0$, the dispersion, OO', in Fig. 4(a) is $-k \tan \theta_M$ in both $\Delta\omega$ and $\Delta 2\theta$ so the slope of the locus is $-135°$ to the $+\Delta 2\theta$ axis. As θ_C increases, the dispersion of the specimen crystal C interacts with the dispersion of crystal M and the slope changes towards $-90°$. When the condition

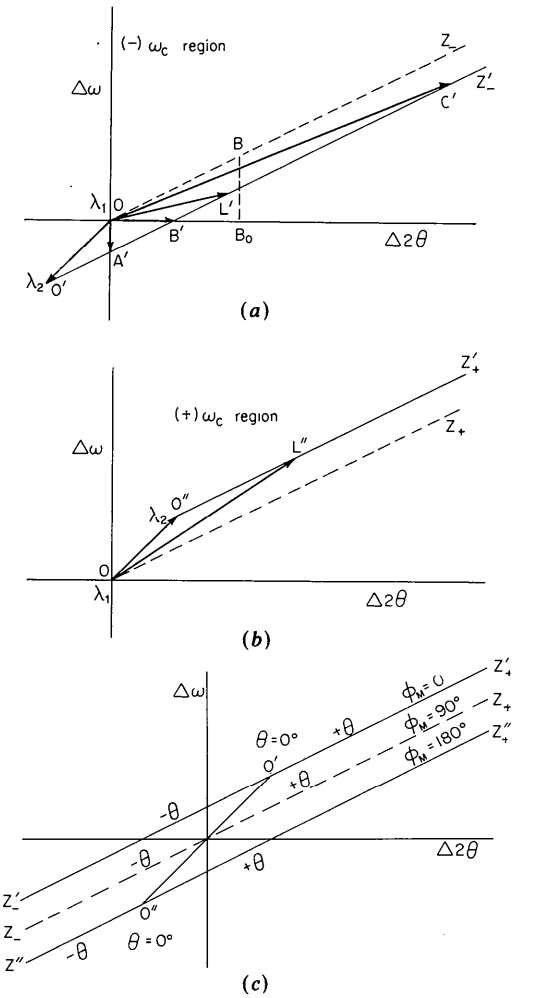

Fig. 4. (a) Wavelength dispersion in the $(-)\omega_C$ region. Diagram of the change of the locus of the wavelength dispersion between λ_1 and λ_2 in $\Delta\omega, \Delta 2\theta^{(0)}$ space in terms of the relationship between θ_C and θ_M given in (3). The local origin in $\Delta\omega, \Delta 2\theta^{(0)}$ space corresponds to the λ_1 peak. OL' represents the locus for a general $k \tan \theta_C$ value; OO', $k \tan \theta_C = 0$; OA', $k \tan \theta_C = (k/2) \tan \theta_M$; OB', $k \tan \theta_C = k \tan \theta_M$; and OC', $k \tan \theta_C > k \tan \theta_M$. The line OZ_- corresponds to the locus for the non-monochromator case. (b) Wavelength dispersion in the $(+)\omega_C$ region. This diagram is based on $(3a)$. OO'' corresponds to $k \tan \theta_C = 0$. OL'' represents a general $k \tan \theta_C$ value. The line OZ_+ corresponds to the locus for the non-monochromator case. (c) The wavelength dispersion diagram for general φ_M values. This diagram is based on (4). For the case where $\varphi_M = 90°$ (and also the non-monochromator case) the locus corresponds to the straight line through the origin at a slope of 1/2 to the $\Delta 2\theta$ axis. Where $\varphi_M = 0°$, the locus limit follows the line $Z'_-O'Z'_+$, O' corresponding to $\tan \theta_C = 0$, $+2\theta(+\omega)$ towards Z'_+ and $-2\theta(-\omega)$ towards Z'_-. Where $\varphi_M = 180°$, the locus limit follows the line $Z''_-O''Z''_+$ parallel to Z_-OZ_+, O'' corresponding to $\tan \theta_C = 0$, $+2\theta(+\omega)$ towards Z''_+ and $-2\theta(-\omega)$ towards Z''_-. The symmetry of the diagram reflects the mutual dependence of φ_M and the sign of 2θ.

$\tan\theta_C = (1/2)\tan\theta_M$ is reached, the slope is $-90°$ exactly and the dispersion corresponds to OA'. Here the dispersion in $\Delta 2\theta$ is zero, *i.e.* all wavelengths in the bandpass λ_1 to λ_2 will arrive at the same point at the detector (or will pass through a fixed narrow slit in front of the detector). The dispersion in respect of $\Delta\omega$ is $-(k/2)\tan\theta_M$. At a further stage as θ_C increases, the slope of the locus moves towards 0° and when the dispersion of M and C are equal, *i.e.* $\tan\theta_C = \tan\theta_M$, the dispersion of the system in respect of $\Delta\omega$ is exactly zero; this corresponds to OB'. This is, of course, the classical condition associated with the two-crystal spectrometer in the so-called parallel condition (Compton & Allison, 1935) (which deals with two extended-face crystals). However, in respect of $\Delta 2\theta$, the dispersion is not zero but is $k\tan\theta_C$ $(= k\tan\theta_M)$. This dispersion in $\Delta 2\theta$ is half of that, $2k\tan\theta_C$, represented by OB_o, appropriate to the non-monochromator case, which would correspond to the point B on OZ_-, Fig. 4(*a*). Further out in θ_C when $\tan\theta_C > \tan\theta_M$, the dispersion, OC', tends towards the non-monochromator dispersion, OZ_-, with slope of $\sim +26{\cdot}6°$ from the lower side, but never quite reaching it. The change in slope of the locus with change in θ_C for the $(-)\omega_C$ region accords with that given by Schoenborn (1983).

(*b*) *The* $(+)\omega_C$ *region*

The situation in this region can be dealt with in a similar manner, Fig. 4(*b*). The relationships derived from consideration of the 'illumination' and 'receptor/transmitter' distributions give the ratio of $\Delta\omega$ to $\Delta 2\theta$ as

$$\frac{\Delta\omega}{\Delta 2\theta} = \frac{k(\tan\theta_C + \tan\theta_M)}{k(2\tan\theta_C + \tan\theta_M)}. \qquad (3a)$$

As in the $(-)\omega_C$ region, the relationship summarized in (3*a*) can be put in diagrammatic form, Fig. 4(*b*). In this region, the dispersion of both M and C is in the same sense. At $\theta_C = 0°$, the dispersion in both $\Delta\omega$ and $\Delta 2\theta$ is $+k\tan\theta_M$ and the slope of the locus is $+45°$ to the $+\Delta 2\theta$ axis. As θ_C increases, the $\Delta\omega$ and $\Delta 2\theta$ dispersion components both increase. There are therefore no critical or interesting conditions encountered involving crossing either $\Delta\omega$ or $\Delta 2\theta$ axes. As $\tan\theta_C$ increases, the dispersion tends, from the upper side, towards but does not reach that corresponding to the non-monochromator dispersion, OZ_+.

Monochromator axis perpendicular to the specimen axis

For the situation where the monochromator crystal axis is perpendicular to that of the specimen crystal, *i.e.* $\varphi_M = 90°$ (Mathieson, 1968), the dispersion of the monochromator is at right angles to that of the specimen crystal (crossed crystals). Hence, for zero-layer (flat-cone) operation, the dispersion in the diffraction plane of the specimen crystal is simply $2k\tan\theta_C$ in respect of $\Delta 2\theta$ and therefore corresponds essentially to the situation with no monochromator (Mathieson, 1983). The dispersion in that plane is symmetrical with respect to $\pm 2\theta_C$. Note, however, that the wavelength range received by the specimen crystal C will depend on what the monochromator crystal transmits (see the following section on *Extended source*).

When a lath-like crystal of widely differing dimensions or one with highly anisotropic fragment structure is used with a perpendicular monochromator, there is a significant possibility that it could pass, at the two extremes, rather different wavelength distributions. Re-orienting to obtain 1D neat profiles (Duisenberg, 1983), which would necessarily lead to spread of the fragment/anisotropy effect along the vertical aperture in front of the detector, would not necessarily avoid the full consequences of this manoeuvre. Even with a spherical crystal, consistent centring is essential.

The wavelength dispersion diagram for general φ_M values

By reference to Fig. 2(*a*) of Mathieson (1968) (which indicates the functional variation of φ_M), the various cases treated above may be unified into one relationship:

$$\frac{\Delta\omega}{\Delta 2\theta} = \frac{k(\tan\theta_C + \cos\varphi_M\tan\theta_M)}{k(2\tan\theta_C + \cos\varphi_M\tan\theta_M)}. \qquad (4)$$

Here we consider the specimen-crystal positive angular region, $+2\theta_C$, as being established according to the Allison–Williams (1930) proposal but specifically for $\varphi_M = 0°$.

Relationship (4) can be presented in a diagrammatic form as in Fig. 4(*c*). It will be noted that the lines for $\varphi_M = 0$ and 180° are related symmetrically, with inversion of $+2\theta_C$ and $-2\theta_C$.

Extended source

Having dealt with cases relating to point sources, we must now consider the situation concerning an extended source emitting radiation that is diffracted from a plane monochromator of mosaic spread μ_M and then incident on a point C (the specimen crystal). To appreciate the parameters of this problem, we make use of the principle of reciprocity in optics. First we consider a point source and determine the size of the resultant extended 'image' along the line SC in Fig. 5 as a function of the mosaic spread μ_M, the depth of penetration of the radiation into the monochromator crystal δ and the wavelength spread $\Delta\lambda = (\lambda_2 - \lambda_1)$. At this stage, some typical numerical

estimates are derived. Then, invoking the reciprocity principle, it is made evident what each part of the extended image (now the extended source) contributes to the beam incident on the point C (now the specimen crystal).

This approach is detailed in Fig. 5 for the symmetrical situation, *i.e.* $SA'_o = A'_oC'_o$. $SA'_oC'_o$ corresponds to the central beam of the μ_M distribution. The outer limits of the distribution for monochromatic radiation are indicated by OA_- and OA_+. For the former, diffraction occurs from the surface plane of the monochromator crystal, M', at A'_- and passes through C'_μ on the line SC'_o. For the latter, diffraction occurs at A'_+ and also passes through C'_μ. Thus, although the mosaic distribution of M may be symmetrical, the 'image' $C'_oC'_\mu$ is asymmetric, the $+(1/2)\mu_M$ and $-(1/2)\mu_M$ components arriving at the same point in the 'image'.

For a plane, M'', below the surface but parallel to it, a similar argument leads to the corresponding 'image', namely $C''_oC''_\mu$, which is equal to $C'_oC'_\mu$ to first order, but displaced. The total 'image' will be compounded of the decreasing contributions from the planes progressively deeper in the monochromator crystal, each contribution being displaced progressively to the right so that the total 'image' has a sharp leading edge with a gradually fading trailing edge.

The discussion in this section has been restricted so far to radiation of one wavelength, λ_1 (say). For radiation of another wavelength, $\lambda_2 > \lambda_1$, the Bragg angle $\theta_2 > \theta_1$ and the corresponding 'image' will lie to the left of that for λ_1.

Since the size of the total 'image' determines the appropriate dimension of the extended source, which will, according to the principle of reciprocity, feed signal into the point C, it is of concern to indicate at this stage the functional dependence of the individual components of the 'image' associated with μ, δ, $\Delta\lambda$ and where possible derive some numerical estimates as a guide. For this purpose, it is assumed that Cu $K\alpha$ radiation is being used and that the monochromator is pyrolytic graphite, the 0002 reflection being used.

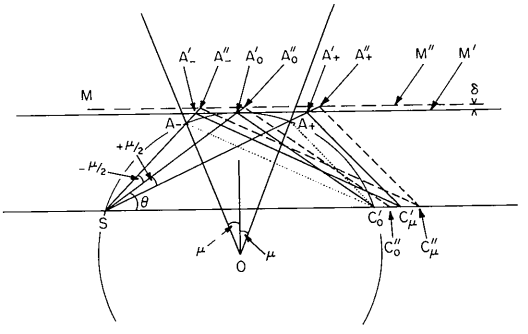

Fig. 5. The relationship of a point source S and the extent of the 'image' at C due to the mosaic spread of the monochromator crystal, μ_M, the depth of penetration into the monochromator, δ, for one wavelength, λ. The disposition of S and C relative to M is essentially symmetrical. $SA'_o(SA''_o)$ is the central beam and $SA'_+(SA''_+)$, $SA'_-(SA''_-)$ the outer limits of the fan of beams due to the mosaic spread. The corresponding diffracted beams from the monochromator surface M' (and a plane below the surface, M'') are $A'_oC'_o(A''_oC''_o)$, $A'_+C'_\mu(A''_+C''_\mu)$ and $A'_-C'_\mu(A''_-C''_\mu)$.

(*a*) *Mosaic spread of M*

So far as the μ_M contribution is concerned, this can be related to the diffraction from any sheet (plane) in the monochromator parallel to the surface. If we consider the surface plane, M', then, from geometrical arguments, based on Fig. 5, it can be shown that

$$C'_oC'_\mu = SC'_o \frac{\sin^2(1/2)\mu_M}{\sin[\theta-(1/2)\mu_M]\sin[\theta+(1/2)\mu_M]} \simeq SC'_o \sin^2(1/2)\mu_M/\sin^2\theta. \quad (5)$$

In normal circumstances, one would be interested mainly in the dimension normal to the X-ray beam, which would correspond to $C'_oC'_\mu \sin\theta = SC'_o \sin^2(1/2)\mu_M/\sin\theta$. If $SC'_o = 400$ mm, $\mu_M = 1°$ and $\theta = 13{\cdot}34°$, then $C'_oC'_\mu = 0{\cdot}46$ mm and the corresponding dimension perpendicular to $A'_oC'_o = 0{\cdot}12$ mm.

(*b*) *Depth of beam penetration*

For a plane that is distant δ below the surface of the monochromator, the leading edge of the 'image' will be at C''_o, which is displaced $2\delta\cot\theta$ along SC from C'_o.

To provide a realistic assessment of how deeply an incident and diffracted beam penetrates into a monochromator crystal, we use experimental data from Calvert, Killean & Mathieson (1975, 1976), which estimated the effective attenuation coefficient (and hence included the effects of n diffraction, *i.e.* extinction).

We calculate the total path that reduces the beam to 1% of the incident intensity. The central beam, with an effective attenuation coefficient of 17·9 cm^{-1}, would penetrate 2·57 mm while beams associated with the outer limits of the mosaic distribution with a coefficient of 9·25 cm^{-1} would penetrate 4·98 mm. The corresponding δ values would be δ(central) = 0·3 mm, δ(wing) = 0·57 mm. So, for δ(central), the displacement at the 'image' would be $0{\cdot}6/\tan\theta = 2{\cdot}53$ mm. As viewed along $A'_oC'_o$, the displacement at the 'image' would be $1{\cdot}14/\tan\theta = 4{\cdot}8$ mm and viewed normal to $A'_oC'_o$ this would be 1·11 mm. The relative depths of penetration of the central and wing beams are indicated in Fig. 6.

(*c*) *Wavelength band*

A change in wavelength from λ to $\lambda+\Delta\lambda$ corresponds to a displacement of $-2\Delta\theta\sec^2\theta/\tan\theta$ to a

first approximation relative to C'_o so, for a dispersion of $\Delta\lambda/\lambda = k$, $C_o(\lambda_1)C_o(\lambda_2)$ corresponds to $-2k\sec^2\theta\, SC'_o$.

If we accept appropriate figures from Mathieson (1984*b*), then $\Delta\lambda = 0{\cdot}012$ Å, $\lambda = 1{\cdot}54$ Å, so $\Delta\lambda/\lambda = 0{\cdot}0078$. (This corresponds to 0·4 pm in front of λ_{α_1}, 0·4 pm behind λ_{α_2} and 0·4 pm between λ_{α_1} and λ_{α_2}.) In that case, the displacement is $-2k\sec^2\theta\, SC'_o = 5{\cdot}9$ mm. Viewed normal to $A'_oC'_o$, this is 1·36 mm.

These items are summarized in Table 1. The components μ_M and δ are two different but inter-related aspects of the monochromator. If μ_M were reduced in size, *i.e.* less mosaic, then the effective attenuation coefficient for the central beam would increase and δ for the central beam decrease. The estimate for the wings would, however, remain unchanged. Basically, for pyrolytic graphite, the depth penetration is of greater significance than the mosaic spread. For monochromator crystals composed of elements of higher absorption, the reverse could be the case.

Invoking the principle of reciprocity, we now invert the roles of source and specimen crystal. If we consider the extended line source, S, as emitting uniformly then, by reference to the treatment above, we can identify those parts of the source associated with the various components μ_M, δ, $\Delta\lambda$, *i.e.* we match the 'illumination' distribution range along S for a given component with the corresponding 'receptor/transmitter' distribution at the point C. Fig. 7 demonstrates the distribution of component ranges along the extended source, S. In Fig. 7(i), as in reality, the components all lie in the line S, whereas in Fig. 7(ii) the various components are displayed at different vertical levels in order to differentiate their intensity contributions and identify their origin. Also, although the λ_1 and λ_2 components correspond to a smooth distribution, they are shown here for clarity as discrete components.

One can see fairly readily from Fig. 7 how limiting the size of the source (by using a focusing assembly or by tilting the X-ray tube to foreshorten the source further) can influence the composition of the radiation arriving at C. For example, if we imagine the source reduced to a length AB, as in Fig. 7, then certain components will not be activated and reach C. Thus, the λ_1 contribution from the surface plane,

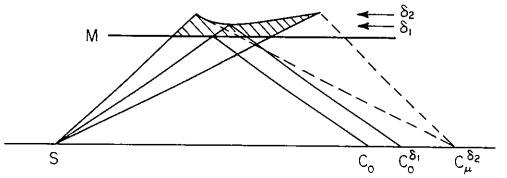

Fig. 6. Illustration, for a typical experimental situation, of the relative depths of penetration, δ_1, δ_2, of the central and wing beams respectively into the monochromator crystal, due to the difference in level of interaction (extinction). The hatched area represents the penetration to the 1% diffraction level.

Table 1. *Size of the source necessary to feed radiation into point C from the various components listed, using the parameters in the text*

Component	Size of the source (mm)	
	(*a*)	(*b*)
μ_M	0·45	0·12
δ	2·53–4·8	0·58–1·11
λ	5·9	1·36

(*a*) along SC and (*b*) perpendicular to $A'_oC'_o$.

M', will be transmitted maximally but those from planes below the surface will progressively decrease, not merely because of the depth, δ, but also due to progressive truncation of the wings of the mosaic distribution. On the other hand, the λ_2 contribution from the surface plane will be zero and will progressively increase its contribution from the wings of the λ_1 distribution as one goes deeper below the surface. So the wavelength distribution reaching C would be modified by the restriction of the source size. Ladell & Spielberg (1966) noted the cut-off effect of reducing source size. The present discussion provides a more detailed appreciation of this effect.

Combining the effect of wavelength dispersion and extended source/monochromator

In previous sections, the effects associated with (*a*) the wavelength dispersion interaction between monochromator and specimen crystals and (*b*) an extended

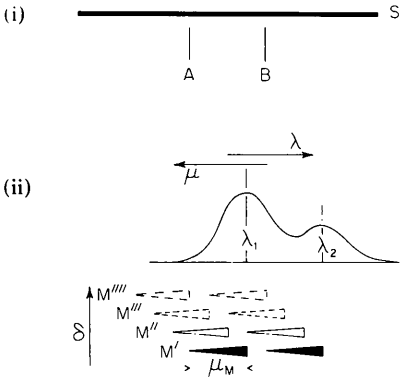

Fig. 7. The relation of the extended source, S, which feeds radiation into the point 'image' C. (i) represents the combination of the components, μ_M, δ, $\Delta\lambda$, into the source, as in reality, in one line. In (ii), the various components from different levels in M are displayed at different vertical positions to demonstrate their displacement along S (in the line CS in Fig. 5). The asymmetric nature of the effective radiation transmission to the image due to the mosaic of M is indicated by the triangular shapes while the break into two components at each M level indicates the two wavelength components. The diagram shows how physical limitation of the size of the source to AB (say) influences the composition of the radiation reaching the point C.

source and monochromator crystal have been treated individually. In this section, the combination of these effects will be considered. It is evident that a complete description of all possibilities is not feasible so some selection is necessary. The combination of effects that is most complex relates to the $(-)\omega_C$ region when $\varphi_M = 180°$ so we shall consider this for different values of $\tan\theta_C$ relative to $\tan\theta_M$.

In Fig. 8, the various situations are illustrated diagrammatically for the ω scan. The specimen crystal mosaicity is μ_C; the combined effects of source/monochromator mosaicity is designated σ/μ_M while the wavelength distribution is designated λ. We assume that the λ distribution involves a doublet λ_1, λ_2, λ_1 being of shorter wavelength and of greater intensity. The loci of the components are detailed in Fig. 8(i) while (ii) attempts to indicate the 2D distribution. Fig. 8(iii) treats the classical so-called parallel case for a vanishingly small source.

Fig. 8 illustrates the situations where (a) $0 < \tan\theta_C < (1/2)\tan\theta_M$; (b) $\tan\theta_C = (1/2)\tan\theta_M$; (c) $\tan\theta_C = \tan\theta_M$ and (d) $\tan\theta_C > \tan\theta_M$. The λ_1, λ_2 components are differentiated, λ_1 being filled in while λ_2 is dotted. Inspection of Fig. 8 shows that the overall shapes of the reflections change considerably as θ_C varies from near 0° to the region where $\theta_C \gg \theta_M$. However, inspection of the diagrams (i) of Fig. 8 indicates that the components μ_C and σ/μ_M are constant in $\Delta\omega, \Delta 2\theta$ angular terms (Mathieson, 1984*a*) and it is the λ component that produces the shape modification. In the low-θ_C-angle region, the orientation of the λ locus changes rapidly and it is this that leads to the significant change in appearance. In this figure, the differentiation of λ_1 and λ_2 allows a more ready appreciation of their relative disposition, which is markedly different from that in the non-monochromator case until one reaches the region $\theta_C \gg \theta_M$.

In respect of this change in shape with change in θ_C, it is clearly evident that, for the conventional wide-aperture procedure, which measures only the 1D profile intensity, $I(\Delta\omega)$, the minimum aperture size required (determined by the range of $\Delta 2\theta$) must be varied continuously with change in θ_C. This is the case whatever the scan procedure used because of the variation in the λ locus, *cf.* the non-monochromator case (Matheison, 1982, 1984*a*). Whether this need for aperture variation has been fully appreciated in X-ray diffractometry in the past is not clear.

The case where $\varphi_M = 0°$ does not require detailing as it is similar to that in Fig. 8(d), except that it approximates to the non-monochromator case from above rather than below.

For the case $\varphi_M = 90°$, the situation is akin to that with no monochromator and is essentially treated by Mathieson (1982, 1984*a*).

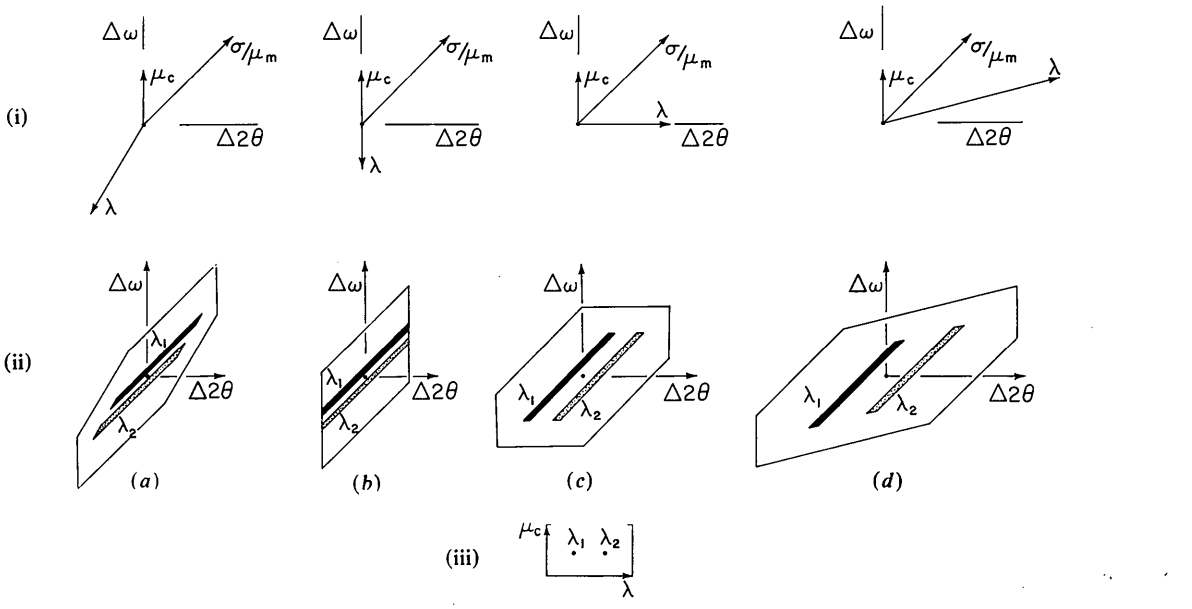

Fig. 8. A diagrammatic representation of the $\Delta\omega, \Delta 2\theta^{(0)}$ intensity distribution, *i.e.* for an ω scan, involving a radiation doublet, λ_1, λ_2 in the case where $\varphi_M = 180°$ and the $(-)\omega_C$ region is considered, for different values of $\tan\theta_C$ relative to $\tan\theta_M$: (a) $0 < \tan\theta_C < (1/2)\tan\theta_M$; (b) $\tan\theta_C = (1/2)\tan\theta_M$; (c) $\tan\theta_C = \tan\theta_M$; (d) $\tan\theta_C > \tan\theta_M$. The specimen-crystal mosaicity is designated μ_C, the source/monochromator mosaicity combination σ/μ_M and the wavelength distribution λ. (i) indicates the relative size and orientation of the μ, σ/μ_M, λ components with respect to the $\Delta\omega, \Delta 2\theta$ axes; (ii) the size of the six-sided box defined by the components, the peak regions of λ_1 and λ_2 being indicated by the filled and dotted bands respectively; (iii) the classical so-called parallel case for a vanishingly small source.

References

ALEXANDER, L. E. & SMITH, G. S. (1962). *Acta Cryst.* **15**, 983-1004.
ALLISON, S. K. & WILLIAMS, J. H. (1930). *Phys. Rev.* **35**, 149-154.
CALVERT, L. D., KILLEAN, R. C. G. & MATHIESON, A. MCL. (1975). *Acta Cryst.* A**31**, 855-856.
CALVERT, L. D., KILLEAN, R. C. G. & MATHIESON, A. MCL. (1976). *Acta Cryst.* A**32**, 648-652.
COMPTON, A. H. & ALLISON, S. K. (1935). *X-rays in Theory and Experiment.* New York: Van Nostrand.
COOPER, M. J. & NATHANS, R. (1967). *Acta Cryst.* **23**, 357-367.
COOPER, M. J. & NATHANS, R. (1968). *Acta Cryst.* A**24**, 481-484; 619-624.
DUISENBERG, A. J. M. (1983). *Acta Cryst.* A**39**, 211-216.
LADELL, J. & SPIELBERG, N. (1966). *Acta Cryst.* **21**, 103-118.
MATHIESON, A. MCL. (1968). *Rev. Sci. Instrum.* **39**, 1834-1837.
MATHIESON, A. MCL. (1978). *Acta Cryst.* A**34**, 404-406.
MATHIESON, A. MCL. (1982). *Acta Cryst.* A**38**, 378-387.
MATHIESON, A. MCL. (1983). *J. Appl. Cryst.* **16**, 572-573.
MATHIESON, A. MCL. (1984*a*). *Acta Cryst.* A**40**, 355-363.
MATHIESON, A. MCL. (1984*b*). *Aust. J. Phys.* **37**, 55-61.
SCHOENBORN, B. P. (1983). *Acta Cryst.* A**39**, 315-321.
WERNER, S. A. (1971). *Acta Cryst.* A**27**, 665-669.
WERNER, S. A. (1972). *Acta Cryst.* A**28**, 143-151.
WILLIS, B. T. M. (1960). *Acta Cryst.* **13**, 763-766.

Acta Cryst. (1985). A**41**, 316-320

Lattice-Dynamical Calculation of Second-Order Thermal Diffuse Scattering in Molecular Crystals

BY A. CRIADO,* A. CONDE AND R. MÁRQUEZ

Departamento de Optica y Sección de Física del Centro Coordinado del CSIC, Universidad de Sevilla, Sevilla, Spain

(*Received* 27 *June* 1984; *accepted* 30 *November* 1984)

Abstract

A computer procedure has been developed to calculate second-order thermal diffuse scattering (TDS) intensity for molecular crystals from lattice-dynamical calculations with an atom–atom potential in the Born–von Kármán formalism. It is applied to monoclinic phenothiazine and different contributions to second-order TDS intensity, acoustic–acoustic, acoustic–optic and optic–optic, are compared. Calculations are also performed in the long-wave approximation allowing for dispersion (LWD) and correction factors of Bragg intensities due to TDS contribution in the LWD approximation are, generally but not always, lower than lattice-dynamical ones; the ratio between LWD and 'exact' factors ranges from 0·4 to 1·4 for reflections considered.

Introduction

In a previous paper (Criado, Conde & Márquez, 1985) we reported a computational procedure to calculate first-order thermal diffuse scattering (TDS) intensity from a lattice-dynamical point of view, using the external Born–von Kármán formalism within the harmonic approximation and a potential function in a pairwise form, where each pair contribution adopts the form: $V(r) = -A/r^6 + B\exp(-Cr)$; A, B and C are constants empirically adjustable. This method was applied to monoclinic phenothiazine, where a proposed potential function model had been successful for calculating the thermal crystallographic parameters (Criado, Conde & Márquez, 1984) and the contribution of inelastic TDS intensity to Bragg reflections measured on a diffractometer by calculating the first-order correction factors for different reflections. Further calculations revealed the influence of first-order TDS intensity over electronic density maps and structural parameters obtained in least-squares refinements. The long-wave limit (Born & Huang, 1968) allowing for dispersion of the acoustic mode frequencies was found to be quite suitable when calculating correction factors because inside the small volumes used to scan the Bragg intensity around a reciprocal-lattice point this limit is usually a good approximation.

Most of the existing programs that correct measured Bragg intensities for thermal diffuse scattering effects (Helmholdt & Vos, 1977; Walker & Chipman, 1970) use the long-wave (LW) approximation taking as the starting point the elastic constants of the crystal and calculating the frequencies and polarization vectors from them, and only very recently (Helmholdt, Braam & Vos, 1983) has the dispersive character of the acoustic modes been taken into account (LWD approximation) using acoustic frequencies obtained from lattice-dynamical calculations.

For the second-order TDS contribution, less effort has been devoted to it, mainly because of the huge amount of computational time required. The programs that consider it adopt the LW approximation (Stevens, 1974) and, in order to reduce the computing

* This work forms part of the Doctoral Thesis.

0108-7673/85/040316-05$01.50